Rhythmic analysis for click train detection and source separation with examples on beluga whales

Olivier Le Bot, Jerome I. Mars, Cedric Gervaise, Y. Simard

Rhythmic analysis for click train detection and source separation with examples on beluga whales

O. Le Bot[1,*], J. I. Mars[*]

University of Grenoble Alpes, GIPSA-Lab, 11 rue des Mathématiques, 38402 Saint Martin d'Hères, France

C. Gervaise[2,*]

University of Grenoble Alpes, Fundation of Grenoble Institute of Technology, 46 Avenue Félix Viallet, 38031 Grenoble Cedex 1, France

Y. Simard[3,*]

Marine Sciences Institute, University of Québec at Rimouski, P.O. Box 3300, Rimouski, Québec G5L-3A1, Canada

Abstract

Passive acoustic monitoring systems are used to study cetaceans through the sounds they produce. Among them, toothed whales emit sequences of acoustic impulses having a rhythmic pattern. As they generally live in pods, click trains from several individuals are often interleaved and recorded together with additional natural or anthropogenic impulsive sources. This paper presents an algorithm that uses the rhythmic properties of odonto-

[*]Corresponding author

Email address: lebotol@gmail.com (O. Le Bot)

[1]also at: Pôle STIC, ENSTA Bretagne (Université Européenne de Bretagne), 2 rue Franois Verny, 29806 Brest Cedex 9, France

[2]also at: University of Grenoble Alpes, GIPSA-Lab, 11 rue des Mathématiques, 38402 Saint Martin d'Hères, France

[3]also at: Maurice Lamontagne Institute, Fisheries and Oceans Canada, P.O. Box 1000, Mont-Joli, Québec G5H-3Z4, Canada

cete click trains for detecting rhythmic impulse trains embedded in other impulse sounds and de-interleaving click trains from simultaneous clicking odontocetes. The contributions of the article are: 1) a method to detect the presence/absence of rhythmic click trains and to characterize the time - Inter Click Interval (ICI) pattern of click trains; 2) an analytical analysis of the performances of this method (jitter, length of click trains); 3) the demonstration of its efficiency on real data with wild beluga whales recorded in Canada.
Keywords: Click train, Inter-click interval (ICI), deinterleaving, time-period analysis, rhythm, marine mammals
PACS: 155, 720

1. Introduction

Sounds produced by marine mammals can be separated in two broad categories: tonal-sounds and clicks. Clicks are very short impulses lasting only tens to hundreds of microseconds [1]. They are produced by all odontocetes (toothed whales) to locate and explore seafloor, submerged obstacles and preys or to communicate. Odontocetes generally emit sequences of several consecutive clicks called *click trains*. The inter-click interval (ICI) ranges from a few microseconds to more than 2 seconds, and varies depending on the species and the activity of the individuals (echolocation, foraging, etc...) [1, 2]. Trains with very short ICI ($\leq$ 20 μs) are called burst pulses [3]. ICI can vary during a train depending on the activity of the individual. As shown by previous studies, there is a random part and a deterministic part in these variations [4, 5, 6, 7].

Tracking the deterministic component of the ICIs within click trains is of great interest to detect and separate rhythmic sources from a mixture of other impulsive sources like snapping shrimps, ice-cracking events or shipping cavitation impulses. This detection and separation task can quickly become difficult when the number of impulsive sources is very large.

Previous methods of detection and separation of odontocete click trains have been based on acoustic descriptors of clicks, such as the amplitude [5], the centroid and peak frequencies [8, 9], the temporal properties [10, 5], high order statistics of the waveform [6, 11]. These methods use either only one or several of these descriptors and range from a simple correlation technics to advanced artificial neural network [12] or multi-hypothesis trackers [13, 14]. Most of them need relatively invariable parameters and/or a-prior training. In a real context, these conditions are not suitable as odontocete clicks have narrow directional beam patterns [1, 2, 15, 16] and most of their acoustic characteristics quickly change or even vanish with the animal orientation. To overcome this difficulty, the direction of arrival (DOA) of the clicks (i.e. the angular position of the sources) can be used as an alternative method to cluster clicks into trains [17, 18]. However, this approach requires the use of an array of several hydrophones and the synchronized reception of each click from each source on all these hydrophones to compute the time difference of arrivals and deduce the DOA of each click. Additionnally, individuals must be spatially distant to achieve a good separation of the clicks based on their DOAs.

Recently, Zaugg *et al.*[19] have proposed a method using a rhythmic analysis and a spectral dissimilarity measure to cluster interleaved sperm whale

clicks into separate click trains. They introduced a metric to estimate the number of subsets of click trains per time unit and apply this metric in a data-mining context.

Unlike previous methods, in our paper we do not use the clicks acoustic descriptors or direction of arrivals but only their time of arrivals (TOA) and a rhythmic analysis algorithm to detect the presence of odontocete click trains. We assume that clicks coming from odontocetes have a rhythmic pattern whereas impulses from other sources have not. Compared to amplitude or spectral characteristics, which can vary greatly during the propagation of the acoustic wave in water, TOAs have the advantage of being less affected by these propagation conditions and by the directivity of the source. Furthermore, TOAs are easy and fast to estimate with traditional click detectors [20, 21, 11].

Classical TOA-based rhythmic algorithms use the autocorrelation of the click trains to build an histogram having peaks located at lags corresponding to ICI-values of the different interleaved trains [22, 23, 24]. It is known that autocorrelation also produces spurious peaks located at values corresponding to multiples of the fundamental ICIs. These subharmonics severely disturb the interpretation of the results. We propose to overcome this problem by using a complex autocorrelation function, which almost completely suppress subharmonics of the autocorrelation while keeping peaks located at the ICI-values of the interleaved trains [25, 26]. Several improvements of this complex autocorrelation have been proposed [27, 28, 29, 30] in a Radar community. Drawing on time-frequency representations Nishiguchi has introduced a time-rhythm (or time-ICI) representation, by computing the com-

plex autocorrelation for windows sliding along the click train, leading to a time-ICI map.

Based on these previous works on the complex autocorrelation, we propose a method capitalizing on the rhythmic properties of odontocete click trains to: 1) detect click trains mixed with other impulsive sources; 2) separate interleaved click trains from several odontocetes emitting simultaneously. We transpose tools based on the complex autocorrelation function and the time-ICI detection to underwater bio-acoustics and passive acoustic monitoring (PAM) methodology. The key question is the behavior of these tools when they are faced with natural signals having their own specific variability rather than regular human-made RADAR signal. The first objective of our paper is to give a whole comprehensive description of this algorithm (from the raw data to the automatic segmentation/detection of time-ICI map). The second objective is to evaluate its analytical performances in regards to its different degree of freedom. The final objective is to show its efficiency on real data of wild beluga.

To our knowledge, only Zaugg *et al.*[19] have used the complex autocorrelation for estimating the ICI of interleaved click trains. Our approach differs on several points. First, our algorithm does not perform preconditioning tests based on spectral dissimilarities between pairs of clicks to suppress some of them. Instead, we consider all click pairs as possible candidates for the rhythm analysis. So, our algorithm comes right after usual click detectors in the processing chain. Second, unlike Zaugg *et al.*'s algorithm, the analysis window is not centered on the detected clicks but slides along the click train as it is usually the case in time-frequency analysis. Third, the time-ICI rep-

resentation obtained at the output of our algorithm has never been used in underwater bio-acoustics and offers several interesting applications.

In the first part of this paper, we present an overview of the complex autocorrelation function and its use with a sliding window to build a time-ICI representation. The second part deals with the performances of the algorithm from a theoretical and analytical point of view. The detectability of a click train depending on parameters such as the length of the train, the jitter and the presence of false alarms, is studied. In this part, we also study the ability of the algorithm to separate interleaved click trains. The third part, uses simulated examples to confirm results obtained in the performance analysis section. The last part shows the efficiency of the proposed method on real data from wild beluga whales recorded at sea.

2. Description of the algorithm

2.1. Overview

Prior to the proposed algorithm, clicks are detected on the waveform with standard click detectors [11, 20, 21] (top part of Fig. 1). Times of local maximum amplitude of the detected clicks are considered as the time of arrival (TOA) of the clicks. This latter list of TOAs is used to perform the rhythmic analysis and separate interleaved click trains. This processing is divided in three steps (Fig. 1).

The first step transforms the list of TOAs to a new representation called *time-ICI map* (Fig. 1). This transformation is based on the complex autocorrelation function, which highlights the fundamental ICIs of the interleaved click trains, while avoiding the subharmonics given by the classical autocorre-

lation. By calculating such complex-autocorrelation in sliding windows along the signal, we obtain a map with the time on the abscissa-axis, the ICI on the ordinate-axis and the amplitude of the autocorrelation on the elevation-axis.

The second step of the algorithm aims to calculate a threshold to identify peaks corresponding to click trains and suppress the possible noise or spurious spike on the time-ICI map. The third step is the thresholding of the time-ICI map to produce the binary time-ICI map more suitable to analyze and distinguish the rhythm of interleaved click-trains.

This method needs 7 input parameters to build the time-ICI representation and calculate the detection threshold (Table 1). Their values have an influence on the performance of the algorithm and are discussed in the performance analysis section. In the next subsections, we detail the signal processing techniques used in each of the three steps. We assume that the list of TOAs is already known so that our analyses do not depend on the click detector performances.

2.2. Complex autocorrelation vs classical autocorrelation

Nelson [25] and Nishiguchi [26] introduced the concept of complex-valued autocorrelation, which automatically suppresses subharmonics that normally appear when calculating the autocorrelation function of rhythmic click trains. The complex autocorrelation function is given by:

$$D(\tau) = \int_{-\infty}^{+\infty} m(t)m(t-\tau)exp(2\pi it/\tau)dt \tag{1}$$

while the classical autocorrelation function is:

$$C(\tau) = \int_{-\infty}^{+\infty} m(t)m(t-\tau)dt \tag{2}$$

where $\tau \in \mathbf{R}^+$ and $m(t)$ represents the click train. Considering that the TOA is the only parameter used to represent each click, this click train can be modeled as a sum of Dirac delta functions:

$$m(t) = \sum_{n=0}^{N-1} \delta(t - t_n) \tag{3}$$

where t_n is the TOA of the n^{th} click, $\delta(.)$ is the Dirac delta function and N is the total number of clicks in the train.

As click detectors usually detect all kind of acoustic impulses, we assume that TOAs of $m(t)$ are a mixture of click trains emitted by odontocetes and others clicks coming from other sources considered as undesirable. Substituting Eq. (3) in Eq. (1) and (2) yields:

$$D(\tau) = \sum_{n=1}^{N-1} \sum_{m=0}^{n-1} \delta(\tau - (t_n - t_m)) exp(2\pi i t_n/\tau) \tag{4}$$

$$C(\tau) = \sum_{n=1}^{N-1} \sum_{m=0}^{n-1} \delta(\tau - (t_n - t_m)) \tag{5}$$

where t_n is the TOA of the n^{th} click and t_m is the TOA of the m^{th} click.

The only difference between the classical and the complex autocorrelation is the use of the complex exponential, which acts like a phase term to eliminate the subharmonics. Mathematical developments [25, 26, 30] explaining subharmonics cancellation can be found in Appendix A.

To illustrate, we have interleaved two simulated click trains whose respective ICIs are equal to 0.0435 s and 0.09 s (Fig. 2a). The complex autocorrelation function of the resulting TOA sequence has two peaks at τ-values equal to the ICI of the two mixed click trains (Fig. 2c). In contrast, the classical

autocorrelation of the mixed click trains shows several peaks located at τ-values corresponding to subharmonics of the fundamental ICIs of each click train (Fig. 2b).

2.3. Time-Rhythm Analysis

2.3.1. Time-ICI map

In this subsection, we describe the *step-1 block* of the proposed algorithm (Fig. 1). To characterize the temporal pattern of the ICI, the complex autocorrelation is performed on sliding windows. This allows: 1) to track rhythm changes due to the odontocete behavior 2) to detect short click-trains mixed with longer click-trains. By analogy to the time-frequency analysis, a time-rhythm analysis is defined by:

$$D(t,\tau) = \int_{s \in W(t,\tau)} m(s)m(s-\tau)exp(2\pi is/\tau)ds \tag{6}$$

where $W(t,\tau) = [t - \nu \times \tau/2, t + \nu \times \tau/2]$ is the time-support of a rectangular sliding window along the interleaved click trains [30]. The window is centered around t and its width is $\nu\tau$ with $\nu \in \mathbf{R}^+$, so that there are always ν periods with ICI equal to τ contained in the window $W(t,\tau)$. This window $W(t,\tau)$ slides with a constant time period, written "*step*" in the rest of this article. The result of the time-rhythm analysis is an image called *time-ICI map*, which is obtained by taking $|D(t,\tau)|$.

To illustrate this point, we present in Fig. 2 (d and e) the time-ICI map of the two previous simulated click trains (Fig. 2a), for both the classical (Fig. 2d) and the complex (Fig. 2e) autocorrelation approaches. This first step of the algorithm requires 6 parameters (see Table 1).

2.3.2. Implementation aspects

To estimate the complex autocorrelation from Eq. (6), the range [τ_{min},τ_{max}] of the ICIs to be investigated is segmented into bins. Values of τ_{min} and τ_{max} are chosen by the user according to the smallest and the highest ICI produced by the target species we want to detect. For beluga whale (target species), $\tau_{min} = 0.001$ s and $\tau_{max} = 0.2$ s.

Initially, the range of ICIs was uniformly divided into small equal intervals [26]. However, evenly spaced bins give a lower density of bins at small ICI values and over fitted bins at larger ICI values [28]. Therefore the resolution of the ICI bins is not constant along the ICI range [τ_{min},τ_{max}]. To keep a constant accuracy and an appropriate constant ICI resolution, Mahdavi proposes to segment the ICI range [τ_{min},τ_{max}] by using a geometric progression [28]. The center of each bin, written τ_k, is therefore given by:

$$\tau_k = r^{k-1}\tau_1 \tag{7}$$

where r is the bin resolution, $k = 1, ..., K$ the bin index and τ_1 the first term of the progression (equal to τ_{min}). As suggested by Mahdavi's work, the resolution r must be slightly higher than 1 to provide a good compromise between the ICI resolution, the number of ICI bins to explore between τ_{min} and τ_{max} and the computational time. In this study, r will be equal to 1.005 (arbitrary choice), giving thus a resolution of 0.5%.

To be able to work with jittered click trains and avoid the reduction of the peaks when ICI values are distributed into many bins, each τ_k value is assigned to a bin b_k centered on τ_k and whose width is given by:

$$b_k = [(1 - \frac{\sigma}{2})\tau_k, (1 + \frac{\sigma}{2})\tau_k] \tag{8}$$

where $\sigma \in \mathbf{R}^+$ represents the upper limit of the jitter. Therefore, each bin has a width equal to $\sigma\tau_k$ and overlaps with its neighboring bins (See Fig. 3). Overlapping helps counterbalancing the jitter effects that tends to smear ICI values into several adjacent bins.

According to this discretization of the ICI range and to the expression used in Eq. (3) to model the click train, we can rewrite Eq. (6) in a discrete form as follow:

$$D(t, \tau_k) = \sum_{\{(t_n - t_m) \in b_k, t_n \in W(t,\tau_k)\}} \exp\left(2\pi i t_n / \tau_k\right) \tag{9}$$

where t_n and t_m are respectively the TOAs of the n^{th} and m^{th} clicks.

2.3.3. Thresholding of the time-ICI map

In this subsection, we introduce an expression to calculate the detection threshold needed in *step-2 block* of the proposed algorithm (Fig. 1). When calculating the modulus of $D(t, \tau_k)$, we obtain a time-ICI map whose amplitude of each pixel with coordinate (t, τ_k) comes from the contribution of all click pairs (t_n, t_m) that satisfies $(t_n - t_m) \in b_k$ and $t_n \in W(t, \tau_k)$. These click pairs can be part of one of the following categories (hypothesis):

- t_n and t_m do not belong to the same click train, i.e. come from two different sources (H_0)
- t_n and t_m belong to the same click train, i.e. come from the same source (H_1)

Since the aim of the algorithm is to detect pulse trains, we want to find a threshold Γ such that for hypothesis H_0: $|D(t, \tau_k)| < \Gamma$ and for hypothesis H_1: $|D(t, \tau_k)| \geq \Gamma$.

Admitting that sources emit click trains independently from each other, then the difference between two successive TOAs is a random process and the number of clicks within a bin b_k follows a Poisson distribution with parameter λ [31]. In practice, a value of λ is calculated in each window $W(t, \tau_k)$ as follow [30]:

$$\lambda = \frac{N^2(t, \tau_k)\sigma}{\nu} \tag{10}$$

where $N(t, \tau_k)$ is the total number of clicks within the sliding window $W(t, \tau_k)$, ν is the constant defined in section 2.3.1 and σ is the constant defined in section 2.3.2.

A relation [30] between the detection threshold Γ, the probability of false alarm P_{fa} and the Poisson parameter λ is proposed:

$$P_{fa} \;=\; 1 - \Gamma \times \int_0^{\infty} exp[\lambda \times (J_0(s) - 1)] J_1(s \times \Gamma) ds \tag{11}$$

where $J_0(.)$ and $J_1(.)$ are respectively the Bessel functions of order 0 et 1. With such relation between λ, P_{fa} and Γ, the threshold adapts to the number of clicks $N(t, \tau_k)$ in each window $W(t, \tau_k)$.

In practice, we are more interested in computing the detection threshold Γ for a given probability of false alarm P_{fa}. Therefore, we numerically solved Eq. (11) with respect to Γ and built a table (or a plot curve) giving Γ for a set of couples (λ, P_{fa}). Fig. 4 gives the evolution of the threshold Γ as a function of P_{fa} and λ. From Fig. 4 we show that the detection threshold increases with λ and decreases when P_{fa} increases.

As an example, to threshold the time-ICI maps (Fig. 2d and 2e), we have saved the value taken by λ in each window $W(t, \tau_k)$ and then found the detection threshold associated to each of them for a P_{fa} equal to 10^{-4}.

Figures 2f and 2g show the results of this thresholding. Again, we can see the advantage of using the complex autocorrelation on Fig. 2g, where no harmonics show up, at the contrary of Fig. 2f.

3. Analytical performances of the algorithm

Performances of the proposed algorithm are affected by the parameters configuration (see Table 1) and by characteristics of the source producing the click train. Critical parameters of the algorithm itself are:

- σ: upper limit of the jitter;
- ν: number of times a given value of ICI is contained in the window $W(t, \tau_k)$;
- Pfa: probability of false alarm of the detector.

Critical parameters relative to the click train itself, i.e. dependent of the source producing the sound and its surrounding environment are:

- w: number of clicks in the train to detect;
- ζ: jitter width of the train to detect;
- q: proportion of extra clicks (i.e. undesirable TOAs) mixed with the click train to detect.

Performance analysis presented in this section is derived from Nishiguchi's analytical formulas [30] and on the statistical properties of our test dataset. In this part we focus on the assessment of:

- detectability of a click train as a function of the parameters cited above;
- minimum ICI difference between two interleaved click-trains allowing their separation.

For a click train to be detected in the window $W(t, \tau_k)$, we recall that the result of the time-ICI map $D(t, \tau_k)$ must satisfy hypothesis H_1 given previously:

$$|D(t, \tau_k)| \geq \Gamma \tag{12}$$

where Γ is the detection threshold obtained numerically from Eq. (11) as explained in section 2.3.3. However, as click trains are affected by a jitter (random variable) the exact distribution of $D(t, \tau_k)$ is unknown. This difficulty is by-passed by computing the signal intensity [30] defined by:

$$Is = \sqrt{E[D^2(t, \tau_k)]} \tag{13}$$

Nishiguchi shows that this signal intensity can be expressed as a function of the critical parameters (σ, ν, w, ζ, q) [30]:

$$I_s^2 = (1 + 2\sigma q)^2 I_0^2 + (q\nu + 2w')\sigma q \tag{14}$$

where $w' = min(w, \nu)$ and I_0 is given by:

$$I_0^2 = w' \frac{1 + sinc(\zeta)}{1 - sinc(\zeta)} - \frac{2sinc(\zeta)[1 - sinc^{w'}(\zeta)]}{[1 - sinc(\zeta)]^2} \tag{15}$$

The detectability condition becomes:

$$I_s \geq \Gamma \tag{16}$$

Poisson distribution coefficient defined by Eq. (10), can also be rewritten as a function of σ, ν, w and q [30] and is now given by:

$$\lambda = \frac{(q\nu + w')^2 \sigma}{\nu} \tag{17}$$

By varying the values of the sextuple (ν, w, q, σ, ζ, P_{fa}), we can determine the conditions for which a click train will be theoretically detectable.

3.1. Detectability of a click train

The question addressed in this section is the detectability of a click train when parameters ($\sigma,\ \nu,\ P_{fa}$) used to built the time ICI map and to calculate the detection threshold are set to fixed value. Therefore, for a given triplet (σ, ν, P_{fa}), we use Eq. (14) and (16) to find values of ($w,\ \zeta,\ q$) allowing click train detection.

In a first simulation, we arbitrarily set ($\sigma,\ \nu,\ P_{fa}$) = ($0.3,\ 10,\ 10^{-4}$) and then calculate the minimum number of clicks (w_{min}), the click train should contain to be detected when $\zeta \in [0\ ,\ 0.4]$ and $q \in \{1,\ 2,\ ...,\ 10\}$. Results of all ($q$, ζ) combinations are summarized in Fig. 5a.

Figure 5a should be read as follow: if $\zeta = 0.02$ and if $q = 4$, then $w_{min} = 7$. This means that the click train should have at least 7 rhythmic clicks to be detected in these conditions ($\zeta = 0.02$, $q = 4$).

A comprehensive analysis of Fig. 5a shows that for values ($\sigma,\ \nu,\ P_{fa}$) chosen above, when $\zeta < 0.16$ the click train should contain at least 6 to 9 clicks to be detected in a mixture of other impulsions. Now if the jitter reaches $\zeta = 0.35$, then we will only be able to detect the click train if it has more than 8 clicks and if $q < 4$. For this same value of ζ, the click train will never be detected if $q > 4$. At last, for the set of parameters ($\sigma,\ \nu,\ P_{fa}$) chosen here, a click train having a jitter $\zeta > 0.4$ will never be detected.

Repeating the above simulation with $\nu = 20$ and the couple ($\sigma,\ P_{fa}$) kept as before, we observe for all combinations of ζ and q, an increase of the minimum number of clicks w_{min} required to detect the click train (Fig. 5b).

In a general manner, as long as ν increases, w_{min} increases as well.

To study the influence of σ, we redo the same simulation with the following parameters: $(\sigma,\ \nu,\ P_{fa}) = (0.2,\ 10,\ 10^{-4})$. Again, we calculate w_{min} for different combinations of ζ and q. Results of this simulation are summarized on Fig. 5c. Comparing Fig. 5a and 5c, show that for a given couple $(q,\ \zeta)$, when σ decreases, more rhythmic clicks are generaly needed in the train to be able to detect it. We notice that for $\sigma = 0.2$, a click train with a jitter $\zeta = 0.35$ mixed to other clicks with a q equal to 4 will not be detectable anymore (Fig. 5c), whereas it was when σ was equal to 0.3 (Fig. 5a).

Synthetization of results from Fig. 5a, 5b and 5c can be expressed as:

- For a given value of the number of extra pluse q, the minimum number of clicks (w_{min}) required to detect a click train increases when ζ increases.

- For a given value of the jitter ζ, the minimum number of clicks (w_{min}) required to detect a click train increases when q increases.

- One can detect a rhythmic click trains whose jitter ζ is slightly higher than the width of the ICI bin b_k given by σ.

These theoretical results should be compared to the characteristics of click trains produced by odontocetes, and particularly to those of belugas we want to detect, in order to see if the conditions of detectability discussed above with the help of Eq. (14) and (16) are compatible with the sound production of this species.

To do, we analyzed an extensive database of beluga's click train, with a focus on the number of clicks produced in each train, on the width of the ICI

range and on the jitter width in between each ICI. Details concerning the database, the material and the method followed to perform this analysis are given in Appendix B. Results of this analysis can be summarized as follow:

- 90 % of beluga's click trains contain more than 6 clicks;
- 90 % of beluga's click trains have a jitter width ζ below 0.25;
- ICI of beluga's click trains ranges in [0.001 s - 0.2 s].

From these real data, we notice that the number of clicks emitted in each click train is compatible with what is required by the proposed algorithm, especially if ν is around 10. Also, the jitter width of beluga's click trains falls within the range of those simulated above. This analysis can help us to choose appropriate values for ν and σ. According to results shown on Fig. 5 and to those obtained in Appendix B, taking $\nu = 10$ and $\sigma = 0.3$, we should be able to detect most of click trains of belugas.

3.2. Minimum ICI ratio to separate two interleaved click trains

One aim of the algorithm is to separate interleaved click trains of simultaneously clicking multiple odontocetes. Each ICI value τ_k is linked to an ICI-bin b_k whose width depends upon the parameter σ (see Eq. (8)), which affects the ICI resolution. A small σ allows differencing two close ICI while a large σ cannot.

Assuming two click trains with respective ICI τ_1 and τ_2 such as $\tau_1 < \tau_2$, the click train with $ICI = \tau_1$ can theoretically be detected up to the ICI-bin $b_k^{'}$ whose lower boundary is given by $\tau_k^{'}(1 - \frac{\sigma}{2}) = \tau_1$. Same, the click train with $ICI = \tau_2$ can theoretically be detected down to the ICI-bin $b_k^{''}$ whose

upper boundary is given by $\tau_k^{''}(1+\frac{\sigma}{2}) = \tau_2$. So τ_1 and τ_2 will be discriminated on the time-ICI map if:

$$\tau_k^{'} < \tau_k^{''} \Longleftrightarrow \tau_1 \frac{1}{(1-\frac{\sigma}{2})} < \tau_2 \frac{1}{(1+\frac{\sigma}{2})} \tag{18}$$

i.e.

$$\tau_1 < \frac{2-\sigma}{2+\sigma}\tau_2 \tag{19}$$

Fortunately in practice, the minimum ICI difference to distinguish two click trains does not need to strictly respect condition of Eq. (19). Indeed, when $\tau_1 \approx \tau_k'(1-\sigma/2)$ the list of TOAs of the click train is given by:

$$[0, \tau_1, 2\tau_1, 3\tau_1, ..., N\tau_1] = [0, \tau_k'(1-\sigma/2), 2\tau_k'(1-\sigma/2), ..., N\tau_k'(1-\sigma/2)] \tag{20}$$

and the complex autocorrelation in bin τ_k' is equal to:

$$D(t, \tau_k') = \sum_{n=0}^{N-1} \exp\left(2\pi i t_n/\tau_k'\right) \tag{21}$$

$$= 1 + \exp\left(2\pi(1-\sigma/2)i\right) + \exp\left(4\pi(1-\sigma/2)i\right) + ... + \exp\left(N \times 2\pi(1-\sigma/2)i\right) \tag{22}$$

Coefficient $(1-\sigma/2)$ acts like a phase-shift term in all exponentials. Because of this phase shift, exponentials are not perfectly in-phase and the amplitude of $|D(t, \tau_k')|$ remains low and below the detection threshold. Same reasoning applies for τ_2 with a phase-shift equal to $(1+\sigma/2)$.

4. Results on simulated data

To validate analytical results obtained in the previous section, we test the proposed algorithm on simulated click trains.

A first simulation is made to check results regarding the minimum number of clicks w_{min} the click train should have to be detectable. We have interleaved a click train containing $w = 370$ clicks having an $ICI = 0.02$ and a jitter width $\zeta = 0.16$ (red curves on Fig. 6) with shorter click trains having an $ICI = 0.035$, a jitter width $\zeta = 0.16$ and containing $w = 5,\ 6,\ 7,\ ...,\ 11$ clicks (purple curves on Fig. 6). With these ICI values, there are about two clicks from first click train in between each pair of clicks from the second train. Thus, for the second click train $q = 2$. The time-ICI map associated to these interleaved click train is built with parameters $\nu = 10$, $\sigma = 0.3$, $P_{fa} = 10^{-4}$ (Fig. 6). With these parameters, according to theoretical results from Fig. (5a), the second click train can only be detected if it contains more than 7 clicks. Figure 6 shows that the click train with an $ICI = 0.035$, i.e. with a $q = 2$, is not detected when $w = 5$, $w = 6$ and $w = 7$. However, when $w \geq 8$ conditions of detectability are reached and click trains are perfectly detected. Click train with $ICI = 0.02$ (in red) has a q almost equal to zero throughout the time and its $w > w_{min}$. Thus it satisfies conditions of detectability and is perfectly detected on the time-ICI map. These observations validate theoretical results from section 3.1.

A second simulation is made with a higher number of interleaved click trains, in order to check the conditions of detectability in a more complicated environment. All click trains have a constant ICI and a jitter width $\zeta = 0.1$. Time-ICI map resulting from this simulation is shown on Figure 7. Click trains are well detected most of the time, as shown by the good agreement between the detection obtained with our algorithm and the ground truth (colored solid lines). However, we see that the more click trains are inter-

leaved, the more missed detections we have. This is particularly the case with the slowest click train ($ICI = 0.12$), for which missed detections appear in time intervals [3 $s, 4$ s] and [6 s, 7.5 s], when the two fastest click trains are present. In time interval [3 s, 7.5 s] the number of extra clicks q inserted between two clicks of the slowest click train is higher than 8. Therefore, we are at the boundaries of the conditions of detectability discussed in section 3.1. As soon as the fastest click trains stops, click train with $ICI = 0.08$ and $ICI = 0.12$ are well detected again.

5. Results on real data

The proposed algorithm is then validated on real data coming from the database studied in Appendix B.

5.1. Results on regular click trains

For this first example, echolocation click trains, i.e. without burst click trains, of wild belugas are interleaved (Fig. 8a). Conditions of separability given by Eq. (19) can again be assessed on this example, as various ratio for $\frac{\tau_1}{\tau_2}$ are met. As above, parameters used to compute the time-ICI map are $\nu = 10$, $\sigma = 0.3$, $P_{fa} = 10^{-4}$. Result of the algorithm is shown on figure 8b (before thresholding) and figure 8c (after thresholding).

In the range [0 s, 20 s] the different interleaved click trains are perfectly detected. Their respective jitter ζ and q are quite low and they all contain a high number w of clicks so that conditions of detectability given by Eq. (14) and (16) are fully respected. Figure 8d also shows the upper and lower ICI bin till where each click train could theoretically be detected. We see there is no overlapping between these boundaries, meaning that separability conditions

(Eq. (19)) are respected, which is confirmed by the binary time-ICI map obtained *in-fine*.

At the contrary, in the range [27 s, 32 s], we have two interleaved click trains with overlapping boundaries. Fortunately, most of the time the complex exponentials are not perfectly in phase for the τ_k values that are common to both click trains, avoiding both tracks to concatenate. Detections of both click trains only merges at 30 s when their ICIs are nearly equal. Most of the time, ICIs of belugas clicking simultaneously are sufficiently different to be perfectly distinguished on time-ICI map.

Interpretation of this time-ICI map can help biologists or bio-acousticians to know that within this 30 s period, at least two animals were present around the hydrophone and that they were using ICI associated to echolocation behavior.

5.2. Results on regular click trains mixed with burst click trains

In this other example, we choose a sequence where an echolocation click train and a burst click train of two belugas from our database are mixed (Fig. 9a). Results obtained with the proposed algorithm are shown on figure 9b and 9c.

While the echolocation click train is alone, in the time interval [28 s, 30.5 s], the detection is nearly perfect and there are no false alarms. We only observe a missed detection around $t = 29$ s due to a too fast increase of the rhythm. At that time, the jitter suddenly increases because the ICI is very different from one click to another (see Train 1 on Fig. 9a). We also notice that the amplitude of the complex autocorrelation is much lower during this rhythm change.

When the burst pulse sound appears ($t = 31.5\ s$), the number of false alarms, which take the form of large black spots on the binary time-ICI map, increases (Fig. 9c). On this example, false alarms appears in all ICI values higher than 0.8 s within the time interval [30.5 s, 33 s]. Since a burst pulse sound is characterized by a very small ICI, we obtain, for the lowest ICI values, a very high number of couples (t_n , t_m) for which t_n belongs to the regular click train and t_m belongs to the burst. The amplitude of the modulus of $D(t, \tau_k)$ (Eq. 6) generated by all these couples (t_n , t_m) is thereby greatly increased. These high amplitudes appears in dark red on figure 9b. Despite the use of an adaptive threshold, this sharp increase can not be compensated.

These false alarms preferably show up in ICI bins for which apparent q is very high (greater than 5 Fig. 9d). This is a real issue in our application field because the dynamics of ICIs produced by all odontocete species is very high. A ratio of 1 to 200 between the smallest and the biggest ICI values emitted is a common thing for most of the species.

6. Discussion

The proposed algorithm only relies on TOAs of the detected clicks, which is a very simple parameter to measure, in comparison to other acoustical parameters like the frequency content for instance. Moreover, as the waveform can suffer of distortions during its propagation through the oceanic canal as well as through the narrow directivity beam pattern of the sound source production mechanism of the animal, amplitude and frequency content of the signal received at the hydrophone can be greatly affected. In contrast, the uncertainty concerning the exact position of the TOA, even with highly

warped waveforms or in low signal to noise ratio conditions, is negligible compared to the size of the ICI (about ten microseconds versus 1 to 100 milliseconds), and so is included within the jitter width. Therefore, TOAs are less affected by the acoustic properties of the source and by the conditions of propagation, which make it a reliable parameter for rhythmic click train detection and click train separation.

The algorithm proposed needs 7 inputs parameters (τ_{min}, τ_{max}, σ, ν, r, *step*, P_{fa}) (see Table 1 for details), which is less than in most of the other algorithms found in the literature. Baggenstoss[6] extracts 28 features for its click association process and Zaugg[19] 13 features. Among the 7 parameters used in our algorithm, the performance analysis showed that only 3 were really critical for the proper functioning of the algorithm (ν, σ and P_{fa}) as they directly impact the results of the complex autocorrelation or the thresholding of the time-ICI map. The respective influences of ν and σ on the click train detectability have been exhaustively examined in section 3. The four other parameters (τ_{min}, τ_{max}, r, *step*) have an impact on the speed of the algorithm, as they directly influence the number of sliding windows used to build the time-ICI map and so the computational cost of the algorithm. This computational cost is also affected by the number of clicks in the sliding windows. Indeed, when the number of clicks increases, the number of couples (t_n, t_m) the algorithm has to examine and associate to an ICI bin increases.

Tests performed on simulated and real data showed that the main difficulty met by our algorithm is its capacity to deal with interleaved click trains having very different rhythms (burst pulse sound mixed with a regular echolocation train) or with single click train mixed with a high number of

false alarms. In both cases, the apparent value of q for the click train we want to detect is very high, typically more than 10.

A solution that we have tried (not presented in this article) to solve this problem is a sequential approach to detect and remove burst pulse sounds before detecting regular echolocation click trains. Results obtained are promising in term of false alarm reduction. Sequence search approach has also been proposed in the literature, either for similar purpose [23] or to finish the process of separation and clustering of clicks belonging to the same train [19]. In this later reference, the sequential search uses the frequency content of the click as a complementary features to obtain better clustering performances. Other features could be used as already suggested in [13, 6, 19].

The algorithm presented in this article works on a single hydrophone, which makes it interesting for long-term monitoring based on sparse autonomous recorders. Its use can then be fruitful for bioacousticians as it improves the detection of odontocetes in areas where other impulsive sources exist. By separating the click train on the time-ICI map and by showing the evolution of the rhythm of each animal with the time, it can be used to study the bio-sonar of these animals. But this time-ICI analysis may also prove to be a complementary method to separation methods based on DOA, that use arrays of multiple hydrophones. Indeed, put our algorithm before the computation of DOAs could help to detect and identify click trains that are common on all hydrophone before associating them for DOA estimation. This might be particularly useful on large aperture array. The processing steps would be as follow: 1) compute the time-ICI map of each hydrophone taken separately; 2) identify spots on the time-ICI map that are common to

all hydrophones 3) calculate DOAs between click trains associated to these identified spots.

7. Conclusion

This paper proposes an algorithm based on a rhythm analysis of the signal to detects rhythmic click-train mixed with non-rhythmic clicks and separates interleaved rhythmic click-trains. We showed that using a complex exponential term in the autocorrelation function was helpful to cancel the subharmonics usually found in the classical autocorrelation. Applying the proposed complex autocorrelation in a window sliding along the interleaved click train allowed to obtain a map representing the ICI of the rhythmic click-trains as a function of the time. An exhaustive analysis of the performances of the algorithm was performed. It showed that the algorithm performs well and is compatible with the properties of click trains of beluga whales recorded in the wild. The approach presented in this paper to analyze odontocete click trains appears to be complementary to the ones found in the literature. Working on a single-hydrophone design, it could also be useful in a multi-hydrophone application context. Possible applications of this method are numerous: detection of odontocete click train in a noisy environment where the signal is polluted by frequent impulses, estimation of the number of odontocetes clicking simultaneously, input for sequential search algorithms that need to know the ICI.

Parameter name	Description
$[\tau_{min}\ \tau_{max}]$	Expected minimum and maximum ICI values
r	Resolution of ICI bins
ν	Number of periods with ICI equal to τ contained in the window W(t,τ)
$step$	Sliding step size of the time window along the pulse train
σ	Upper limit of the jitter in ICI bins b_k
P_{fa}	Targeted probability of false alarm

Table 1: algorithm parameters to built the time-ICI map

percentile	10^{th}	20^{th}	30^{th}	40^{th}	50^{th}	60^{th}	70^{th}	80^{th}	90^{th}	100^{th}
number of click per train	6	9	15	21	29	40	55	76	120	293
ICI (s)	0.013	0.029	0.034	0.038	0.044	0.049	0.057	0.068	0.093	0.22
ICI jitter given by Eq. (B.1) (%)	0.17	0.37	0.6	0.94	1.4	2.0	3.1	5.2	12.4	100

Table 2: Percentiles of the characteristics of the manually annotated wild beluga click trains recorded in Canada by Fisheries and Oceans Ministery. Total number of clicks in the dataset: 11881. Number of ICI values: 11633.

Appendix A. Subharmonic Suppression

In this appendix, we demonstrate the effect of the complex exponential term on the suppression or reduction of the subharmonics. Let's consider the particular case of a pulse train coming from a single source, without any additional undesirable clicks. TOAs for this rhythmic source are given by the following equation:

$$t_i = i \times ICI \tag{A.1}$$

where ICI is the rhythm at which clicks are emitted by the source and $i = 1$, ..., N is the click index.

With such TOA expression, Eq. (4) becomes

$$D(\tau) = (N-1)\delta(\tau - ICI) + \sum_{l=2}^{N-1} \delta(\tau - l \times ICI) \frac{sin(N\pi/l)}{sin(\pi/l)} e^{\pi i(N+1)/l} \tag{A.2}$$

The first term on the right hand side of Eq. (A.2) represents the contribution of impulses located at the fundamental ICI ($\tau = ICI$) and its modulus is $N - 1$. The second term represents the contribution of impulses located at integer multiples of the ICI, i.e. $\tau = l \times ICI$, and gives the amplitude of subharmonics. For $l \in$ [2 ; N-1] the amplitude of the l^{th} subharmonic is given by:

$$\Big| \frac{sin(N\pi/l)}{sin(\pi/l)} \Big| \tag{A.3}$$

In the case of a single pulse train, the classical autocorrelation function gives the following result:

$$C(\tau) = \sum_{l=1}^{N-1} (N-l)\delta(\tau - lp) \tag{A.4}$$

The amplitude of the l^{th} subharmonic is $N - l$.

For a click train having $N = 100$ clicks, we calculate the amplitude of all subharmonics ($l \in [2, ..., 100]$) for both complex and classical autocorrelation using Eq. (A.3) and Eq. (A.4) respectively (Fig. 10). We clearly see that for most of the subharmonics, the amplitude of the complex autocorrelation is much lower than the amplitude of the classical autocorrelation. They have the same amplitude only when the index of the harmonic l becomes very close to N. Changing the number of clicks N only alters the amplitude of both the complex and the classical autocorrelation by a common scale factor.

Appendix B. Click train production by beluga whales

Numerous publications [2, 8, 15] and books [1, 3] describe the characteristics of bio-sonar clicks produced by odontocetes, in term of source level, frequency content, directivity or ICI. However, little is known about properties of click trains taken in their entirety.

To properly tunes the proposed algorithm parameters and assess its operating conditions, it is necessary to know the characteristics of the click trains of the particular species we want to detect. Among the characteristics of interest, we can cite the range of ICI produced by the species, the number of click per train or the distribution of the jitter, that will directly affect the proper functioning of the algorithm and the tuning of its parameters.

Appendix B.1. Materials and methods

We therefore studied a large amount of data of beluga whale (*Delphinapterus leucas*) click trains recorded in August 2011 in the Cumberland sound, southern Baffin Island (Lat. 66.577°N, Long. 67.481°W, Canada).

During the experiment, the signal of a hydrophone (High Tech Inc., Gulport, MS, USA) was amplified by 25 dB before to be recorded by an IOtech DaqBoard3000/USB having a 16-bit resolution, connected to a personal computer (PC). A sampling frequency of 300 kHz was used for recording the hydrophone signal under a wave format.

To analyze click-train properties, 248 click trains containing a total of 11881 clicks were manually annotated by looking at the waveform and the spectrogram. Here, we call *click train*, a set of consecutive clicks emitted by the same beluga. Only trains for which clicks could be associated to a single individual without any doubt were selected. The TOA of each click was assigned to the signal sample corresponding to the peak amplitude of the click. The list of TOAs corresponding to each annotated click train was then used to estimate the successive ICIs and extract the statistical and serial characteristics:

- number of clicks per train;
- ICI;
- average relative jitter.

Appendix B.2. Results

Appendix B.2.1. Beluga click train statistics

One of the main parameters affecting the performances of the proposed algorithm is the number of clicks in each click-train, which should exceed a minimum threshold (see below). The probability density function (PDF) and the cumulative distribution function (CDF) of the number of clicks per

train for the 11881 clicks show that the number of clicks per click train ranges from few clicks, typically 4 or 5, to more than 250 clicks (Fig. 11a). Overall, 90 % of the click trains contain more than 6 clicks, 70 % have more than 15 clicks and 50 % have more than 29 clicks (Table 2).

A second parameter to consider when tuning the algorithm is the range of ICI of interest, i.e. the interval $[\tau_{min}, \tau_{max}]$ in which the complex autocorrelation will be computed, as already discussed in section 2.3.2. ICIs of the annotated database are mainly distributed between 0.004 and 0.2 s (Fig. 11b). More than 60% of them are between [0.025 s, 0.07 s] and 80% between [0.015 s, 0.092 s] (Table 2). A peak at ICI $\leq$ 0.01 s corresponds to clicks belonging to burst pulse sounds. Burst pulses represent less than 10% of the annotated clicks. The ICI range setting can be done with the help of the PDF of Fig. 11b. We recall that for all results for belugas shown in this paper we took $\tau_{min} = 0.001\ s$ and $\tau_{max} = 0.2\ s$

The distribution of the ICI values depends on the number of clicks in the train (Fig. 11c). Short click trains generally have higher ICI values and a larger variability. The ICI distribution narrows down and the median ICI decreases with increasing number of clicks per train.

Appendix B.2.2. Rhythmic properties of beluga click trains

The proposed algorithm requires that clicks follow a rhythmic pattern. To validate this assumption, we examined the relationships between the ICI of the n^{th} and the $(n+1)^{th}$ pairs of clicks of each annotated click train. Results show that the ICI of the n^{th} and the $(n+1)^{th}$ click pairs are linearly related (Fig. 11d). The linear relation is given by: $ICI(n) = ICI(n+1)$. The coefficient of determination, which is a real value indicating how well data fit

a linear model, is equal to 0.86, confirming the linear relation from one ICI to the next one. The hypothesis that clicks are not randomly produced but follow a rhythmic pattern is therefore validated. However, the residual from the linear regression increases with increasing ICI. We evaluate the average relative jitter between all n^{th} and $(n+1)^{th}$ ICI pairs of the database as follow:

$$\delta_{ICI_1} = \Big|\frac{ICI(n+1) - ICI(n)}{0.5 \times [ICI(n) + ICI(n+1)]}\Big| \tag{B.1}$$

Although the jitter can reach high values, it is below 10 % most of the time (Table 2). The median is 1.4 %, the 80^{th} percentile is 5.2 % and the 90^{th} percentile is 12.4 %. Ignoring burst pulse sounds, the mean of the average relative jitter per ICI decile increases with increasing ICI (Fig. 11e, Table 2).

In summary, the useful click characteristics for the tuning and the performance analysis of the algorithm are:

- ICI range: $[\tau_{min}, \tau_{max}]$ = [0.001 s , 0.2 s]
- Number of click per train: [4 , 293]
- Jitter width (i.e. $2\times\delta_{ICI_1}$): [0 0.3]

Acknowledgement

The authors wish to thank Marianne Marcoux and Steve Ferguson of Fisheries and Oceans Canada for collecting data. Research National Agency (ANR) for funding this work, Grant No. ANR-12-ASTR-0021-03 "MER CALME". We thank two anonymous reviewers for very valuable comments on a previous draft of this manuscript.

References

[1] W. W. L. Au, The SONAR of Dolphins, Springer, New York, 1993.

[2] W. M. X. Zimmer, M. P. Johnson, P. T. Madsen, P. L. Tyack, Echolocation clicks of free-ranging cuvier's beaked whales (ziphius cavirostris), J. Acoust. Soc. Am. 117 (2005) pp. 3919–3927.

[3] W. Au, M. Hastings, Principles of Marine Bioacoustics, Springer, New York, 2008.

[4] M. André, C. Kamminga, Rhythmic dimension in the echolocation click trains of sperm whales: a possible function of identification and communication, J. Mar. Biol. 80 (2000) pp. 163–169.

[5] P. Lepper, N. Dumortier, K. Dudzinski, S. Datta, Separation of complex excholocation signal trains from multiple bio-sonar sources, in: Proceedings of the International Conference on Underwater Acoustic Measurements: Technologies and Results, 2005, pp. 913–918.

[6] P. Baggenstoss, Separation of sperm whale click-trains for multipath rejection, J. Acoust. Soc. Am. 129 (2011) pp. 3598–3609.

[7] W. M. X. Zimmer, Passive acoustic monitoring of cetaceans, University press, 2011.

[8] D. S. Houser, D. A. Helweg, P. W. Moore, Classification of dolphin echolocation clicks by energy and frequency distribution, J. Acoust. Soc. Am. 106 (1999) pp. 1579–1585.

[9] J. Starkhammar, J. Nilsson, M. Amundin, S. A. Kuczaj II, M. Almqvist, P. H. W., Separating overlapping click trains originating from multiple individuals in echolocation recordings, J. Acoust. Soc. Am 129 (2011) pp. 458–466.

[10] R. Bahl, T. Ura, T. Fukuchi, Towards identification of sperm whales from their vocalizations, Seisan Kenkyu 54 (2002) pp. 409–413.

[11] C. Gervaise, A. Barazzutti, S. Busson, Y. Simard, N. Roy, Automatic detection of bioacoustics impulses based on kurtosis under weak signal to noise ratio, Appl. Acoust. 71 (2010) pp. 1144–1163.

[12] G. E. Ioup, J. W. Ioup, L. A. Pflug, A. M. Tashmukhambetov, N. A. Sidorovskaia, Acoustic identification of beaked and sperm whales, J. Acoust. Soc. Am 122 (2007) pp. 3003.

[13] O. Gerard, C. Carthel, S. Corraluppi, Estimating the number of beaked whales using an mht tracker, in: Proc. of New Trends for Environmental Monitoring using Passive Systems (PASSIVE'08), 2008.

[14] O. Gerard, C. Carthel, S. Corraluppi, Classification of odontocete buzz clicks using a multi-hypothesis tracker, in: Proc. of OCEANS 2009, IEEE Int. Conf., 2009, pp. 1–7.

[15] W. M. X. Zimmer, J. Harwood, P. L. Tyack, M. P. Johnson, P. T. Madsen, Passive acoustic detection of deep-diving beaked whales, J. Acoust. Soc. Am. 124 (2008) pp. 2823–2832.

[16] W. W. L. Au, B. Branstetter, P. W. Moore, J. J. Finneran, The

biosonar field around an atlantic bottlenose dolphin (tursiops truncatus), J. Acoust. Soc. Am. 131 (2012) pp. 569–576.

[17] P. Giraudet, H. Glotin, Real-time 3d tracking of whales by echo-robust precise tdoa estimates with a widely-spaced hydrophone array, App. Acoust. 67 (11-12) (2006) pp. 1106–1117.

[18] F. Caudal, H. Glotin, Multiple real-time 3d tracking of simultaneous clicking whales using hydrophone array and linear sound speed profile, in: Acoustics, Speech and Signal Processing, 2008 (ICASSP 2008). IEEE Int. Conf., 2008, pp. 2441–2444.

[19] S. Zaugg, M. van der Schaar, L. Houegnignan, M. André, Extraction of pulse repetition intervals from sperm whale click trains for ocean acoustic data mining, J. Acoust. Soc. Am 133 (2012) pp. 902–911.

[20] S. Kay, Fundamentals of statistical signal processing Volume 2: Detection Theory, Prentice Hall, 1998.

[21] V. Kandia, Y. Stylianou, Detection of sperm whale clicks based on the teager-kaiser energy operator, App. Acoust. 67 (2006) pp. 1144–1163.

[22] R. Wiley, Electronic intelligence: The analysis of radar signals, Artech House Edition, Boston 2nd (1993) pp. 177–188.

[23] H. Mardia, New techniques for the deinterleaving of repetitive sequences, in: IEE Proc. Radar and Signal Processing, Vol. 136, 1989, pp. 149–154.

[24] D. Milojevic, B. Popovic, Improved algorithm for the deinterleaving of

radar pulses, in: IEE Proc. Radar and Signal Processing, Vol. 139, 1992, pp. 98–104.

[25] D. Nelson, Special purpose correlation functions for improved signal detection and parameter estimation, in: Acoustics, Speech, and Signal Processing, 1993 (ICASSP 1993), IEEE Int. Conf., Vol. 4, 1993, pp. 73–76.

[26] K. Nishiguchi, M. Kobayashi, Improved algorithm for estimating pulse repetition intervals, IEEE Trans. Aero. Elec. Sys. 36 (2000) pp. 407–421.

[27] G. Guo, Y. Mao, J. Han, X. Qing, An improved algorithm of pri transform, in: WRI Global Congress on Intelligent Systems., IEEE Int. Conf., Vol. 3, 2009, pp. 145–149.

[28] A. Mahdavi, A. Pezeshk, A fast enhanced algorithm of pri transform, in: Proc. Int. Symp. Parallel Computing in Electrical Engineering (PARELEC), IEEE Int. Conf., 2011, pp. 179–184.

[29] X. Zhao, H. Wang, C. Yang, H. Wu, A new pri transform for the deinterleaving of radar pulses, App. Mech. and Mat. 109 (2012) pp. 528–531.

[30] K. Nishiguchi, Time-period analysis for pulse train deinterleaving, Transaction of the Society of Instrument and Control Engineers E-4 (2005) pp. 68–78.

[31] A. Papoulis, Probability, random variables and stochastic processes, 3rd Edition, McGraw-Hill, New York, 1991.

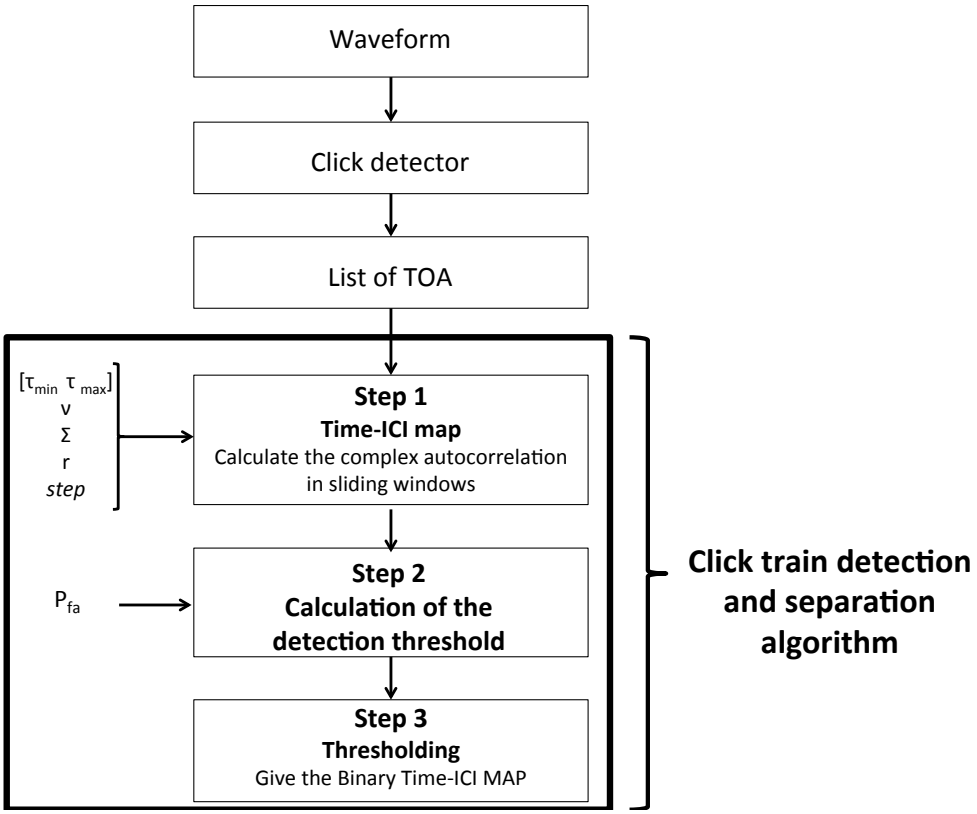

Figure 1: Signal processing steps of the proposed algorithm. The seven parameters needed to build the time-ICI map and perform the detection of the click trains are: $[\tau_{min}\ \tau_{max}]$: the expected minimum and maximum ICI values; r: the resolution of ICI bins; ν: the number of periods with ICI equal to τ contained in the window W(t,τ); *step* the size of the sliding step of the time window along the pulse train; σ: the upper limit of the jitter in ICI bins b_k; P_{fa}: the targeted probability of false alarm.

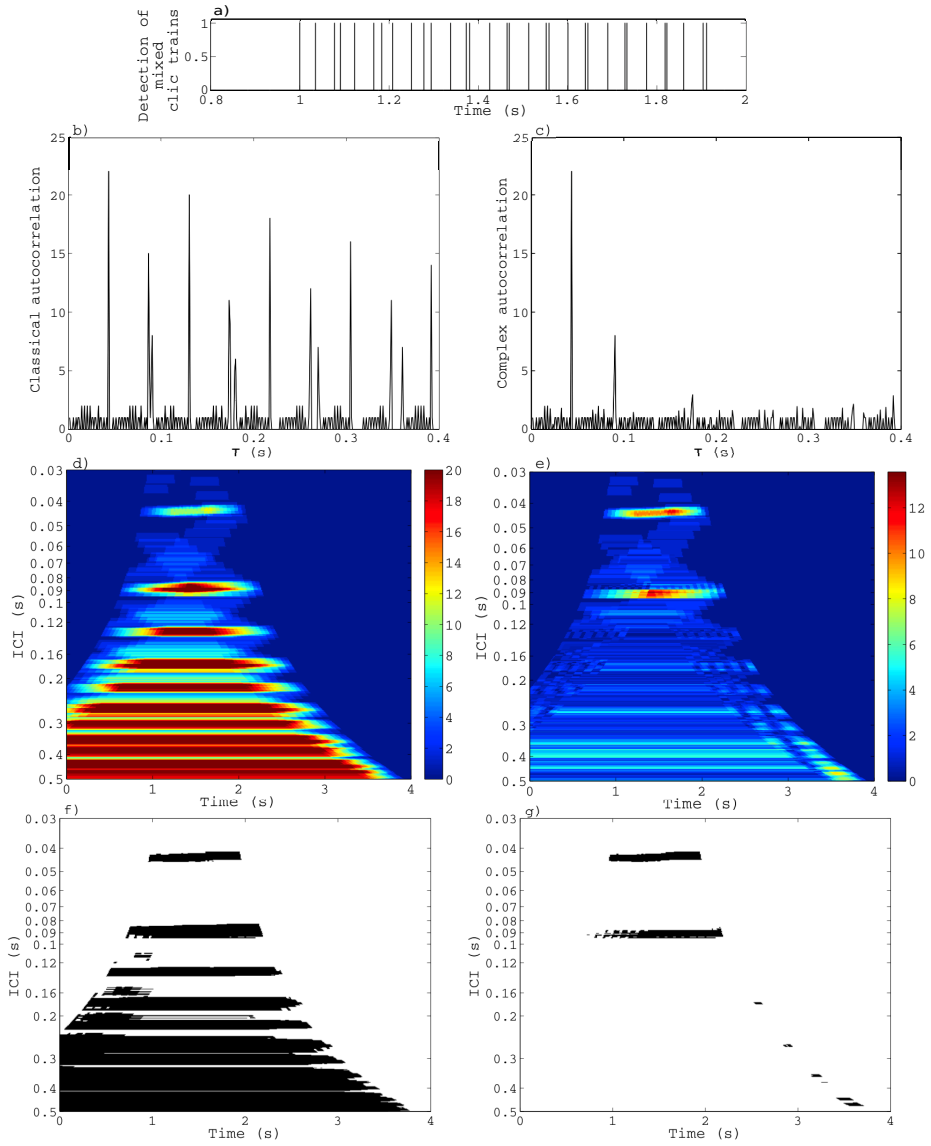

Figure 2: (a) Example of two interleaved simulated click trains as it would be received by a hydrophone. Respective ICIs are 0.09 s and 0.0435 s ; b-g) Output of the steps of the proposed algorithm using the complex autocorrelation (right column) and comparison with the classical autocorrelation (left column); b-c) Results of the classical and complex autocorrelation for mixed click trains from a); d-e) Step 1: Corresponding time-ICI map; f-g) Step 3: Corresponding binary time-ICI map. The inverted direction of the ordinate axis in d-g are consistent with the usual frequency direction of the spectrograms.

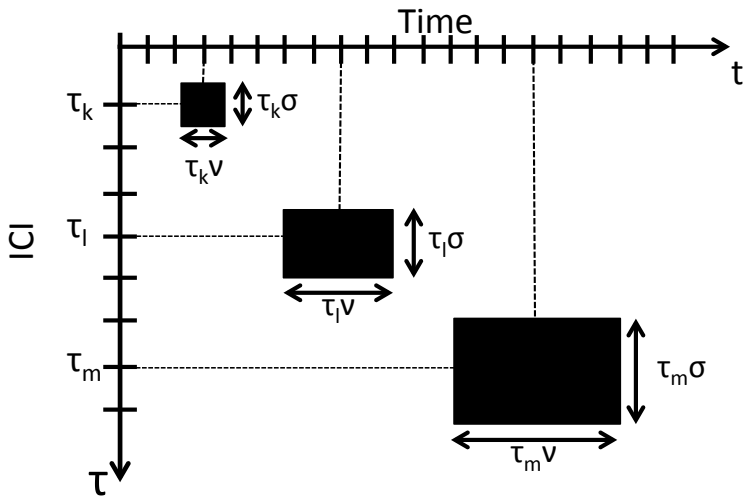

Figure 3: Implementation aspects of RACESS algorithm. The drawing represents how the width of the sliding window and the width of the ICI-bin evolves depending on the value of the ICI τ on the time-ICI map. When the ICI τ increases, the width of the ICI-bin increases proportionally to σ. When the ICI τ increases, the length of the sliding windows increases proportionally to ν.

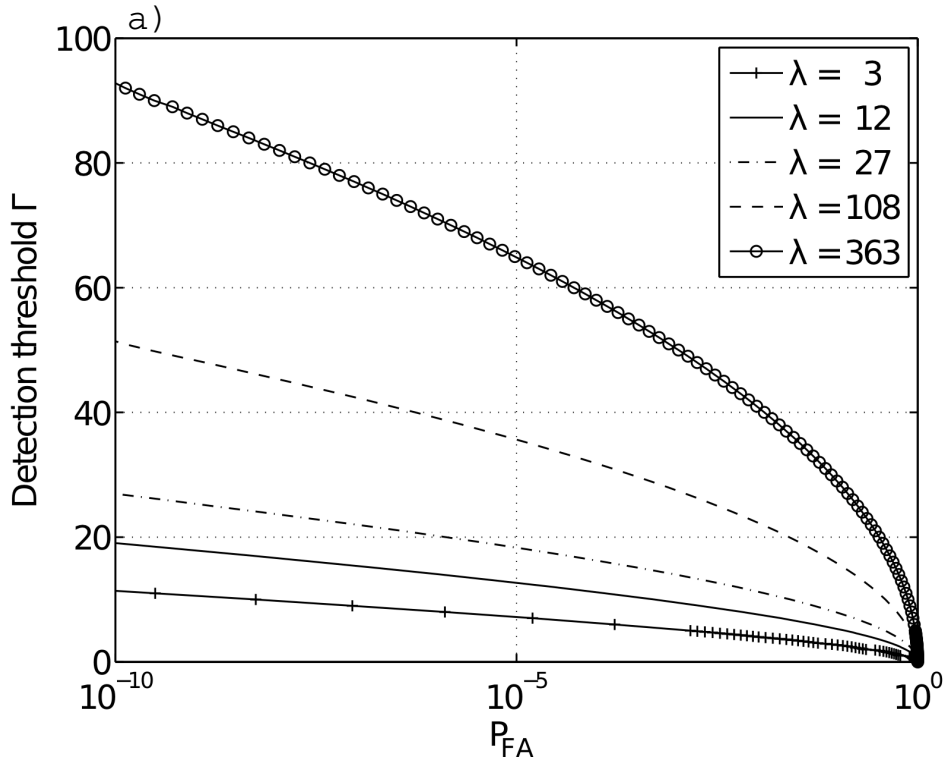

Figure 4: Detection thresholds as a function of the probability of false alarm (P_{fa}) and the Poisson parameters λ, given by Eq. (11).

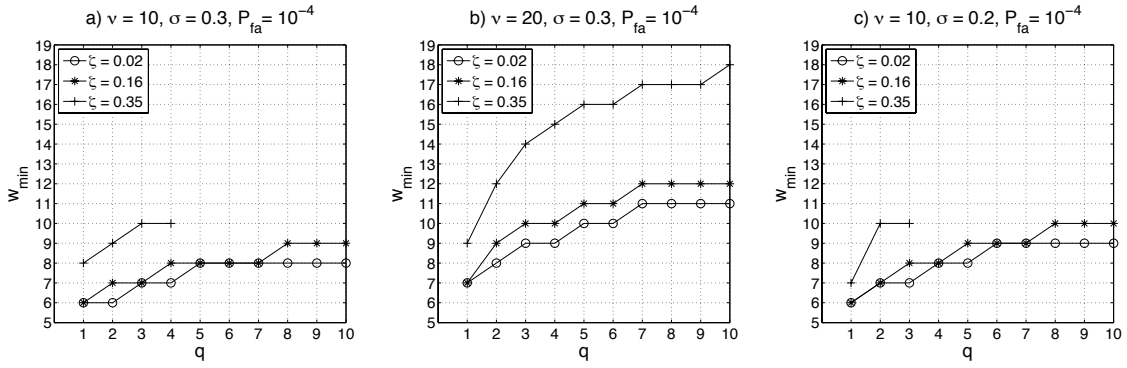

Figure 5: Theoretical conditions of detectability expressed in term of minimum length of detectable click train (w_{min}) as a function of the proportion of extra pulse q and for jitter width $\zeta = 0.02$, $\zeta = 0.16$ and $\zeta = 0.35$. Parameters used to built the time-ICI map are: a) (ν, σ, Pfa)=(10, 0.3, 10^{-4}); b) (ν, σ, Pfa)=(20, 0.3, 10^{-4}); (ν, σ, Pfa)=(10, 0.2, 10^{-4}).

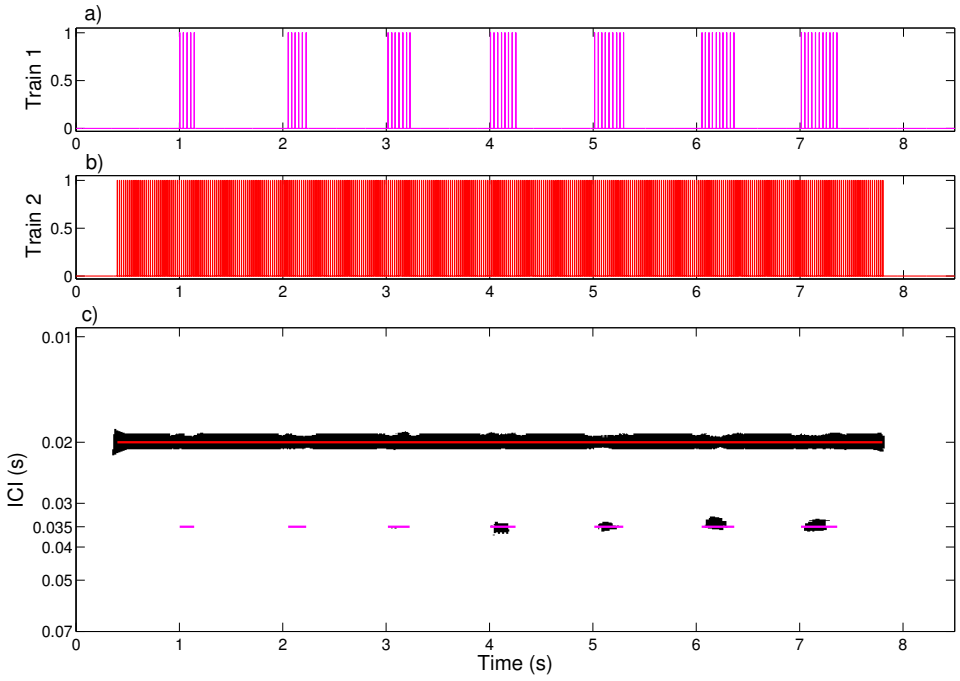

Figure 6: (Assessment of the theoretical conditions of detectability with simulated data. a) First click train (purple curve) is sub-divised in 7 parts. Within each part the ICI= 0.035 s and jitter width is $\zeta = 0.16$. Number of clicks within each sub-part is respectively: 5, 6, 7, 8, 9, 10 and 11. b) Second click train (red curve) has an ICI=0.02 s, a jitter width $\zeta = 0.16$ and $w = 370$ clicks. c) Time-ICI map of two interleaved click trains. Thin colored lines on the time-ICI map correspond to the instantaneous ICI (ground truth).

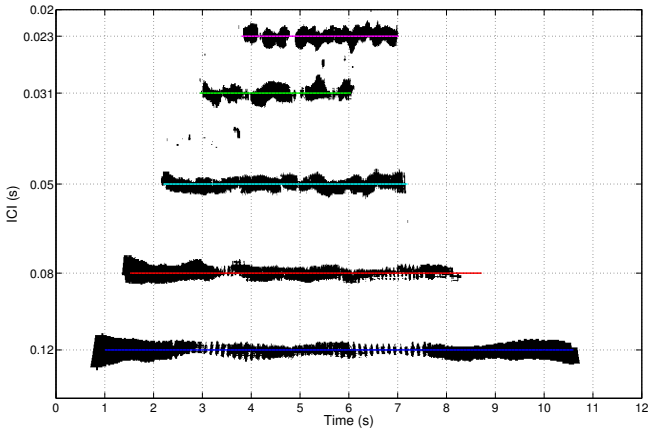

Figure 7: Time-ICI map of five interleaved simulated click trains. Thin colored lines correspond to the instantaneous ICI (ground truth).

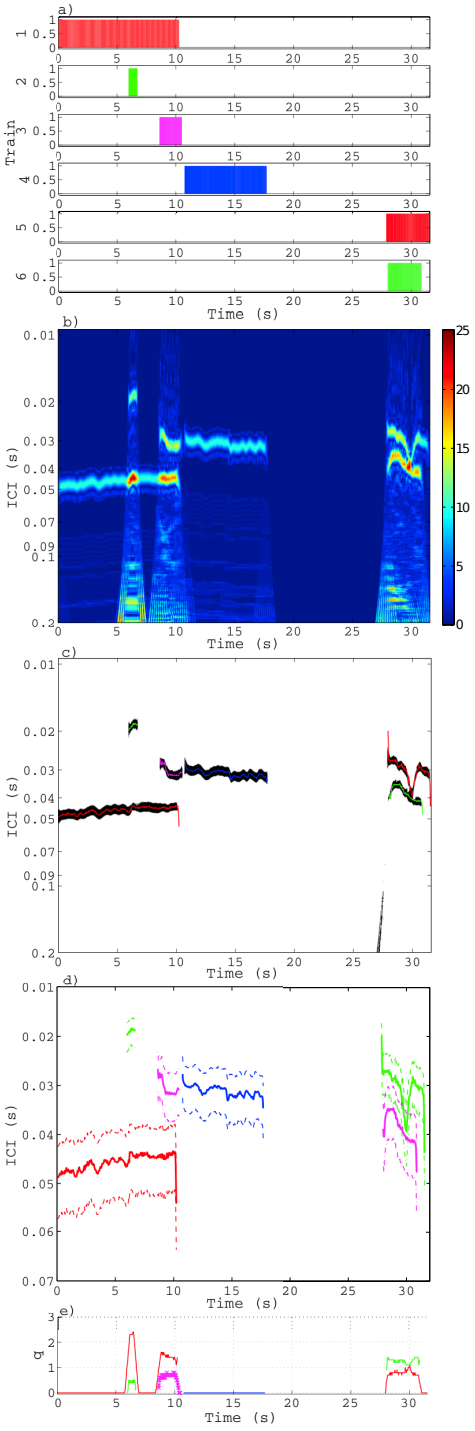

Figure 8: Results of the algorithm for six interleaved wild beluga click trains. a) Sequence of the six click trains. b) Time-ICI map. c) Binary time-ICI map (bold line). ICI measured manually (thin line). d) Instantaneous rhythm of interleaved click train (solid line) and their respective lower and upper ICI-bin limit (dashed line). e) q the average number of extra pulses mixed with the train to detect.

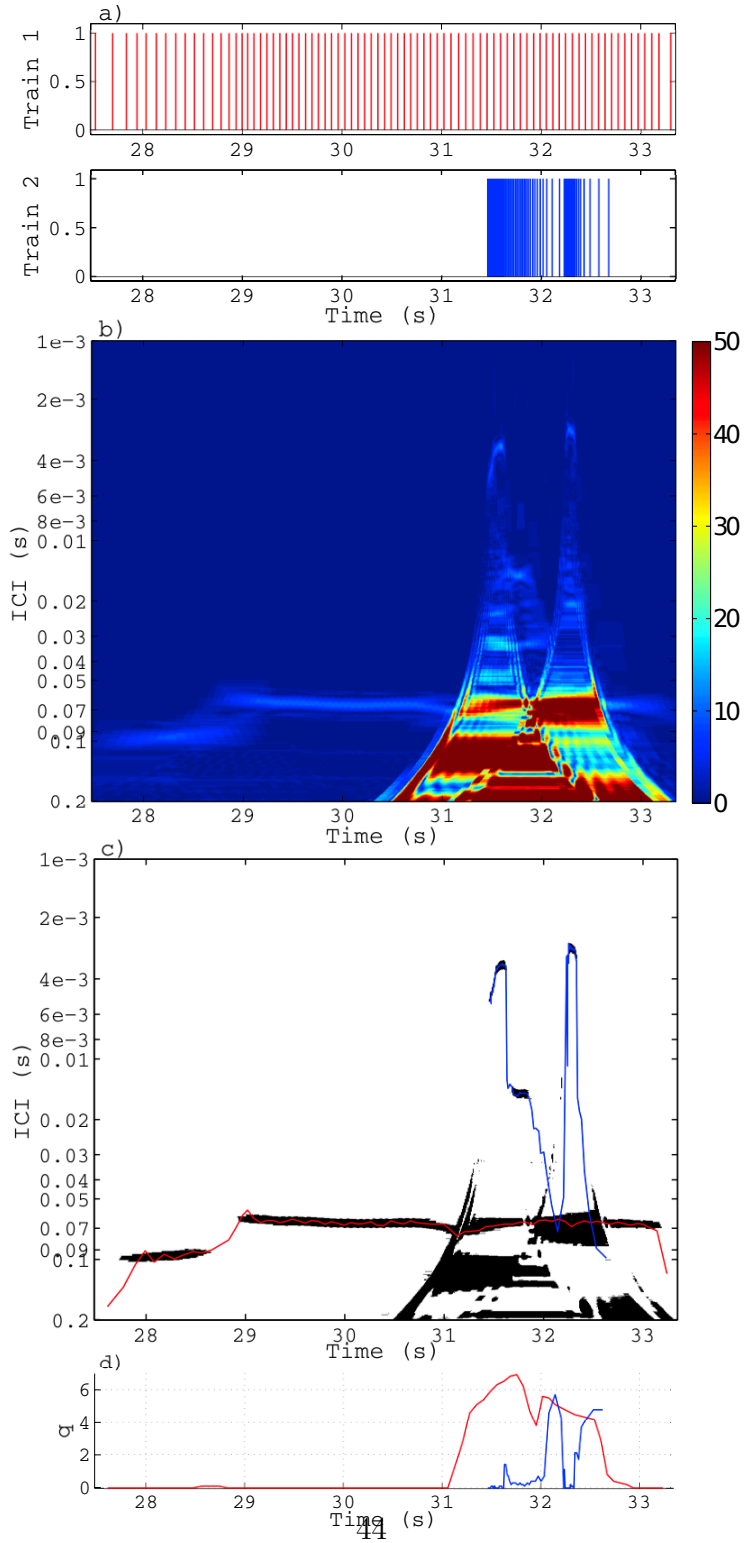

Figure 9: Results of the algorithm for interleaved beluga burst pulse train and click train. a) Clicks time of arrival. b) Time-ICI map. c) Binary time-ICI map (bold line). ICI measured manually (thin line). d) q the average number of extra pulses mixed with the train to detect.

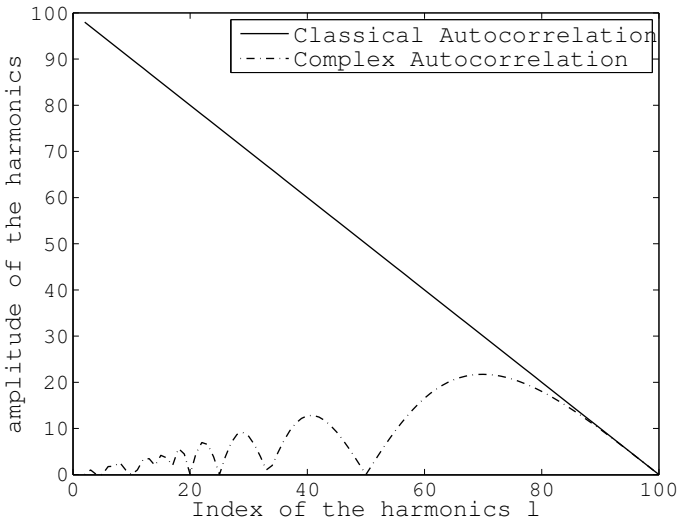

Figure 10: Amplitude of the harmonics (the classical autocorrelation - solid line, the complex autocorrelation - dashed line)when the number of clicks in the train is N=100. For most subharmonics l, the amplitude obtained with the complex-autocorrelation is much lower than with the classical-autocorrelation.

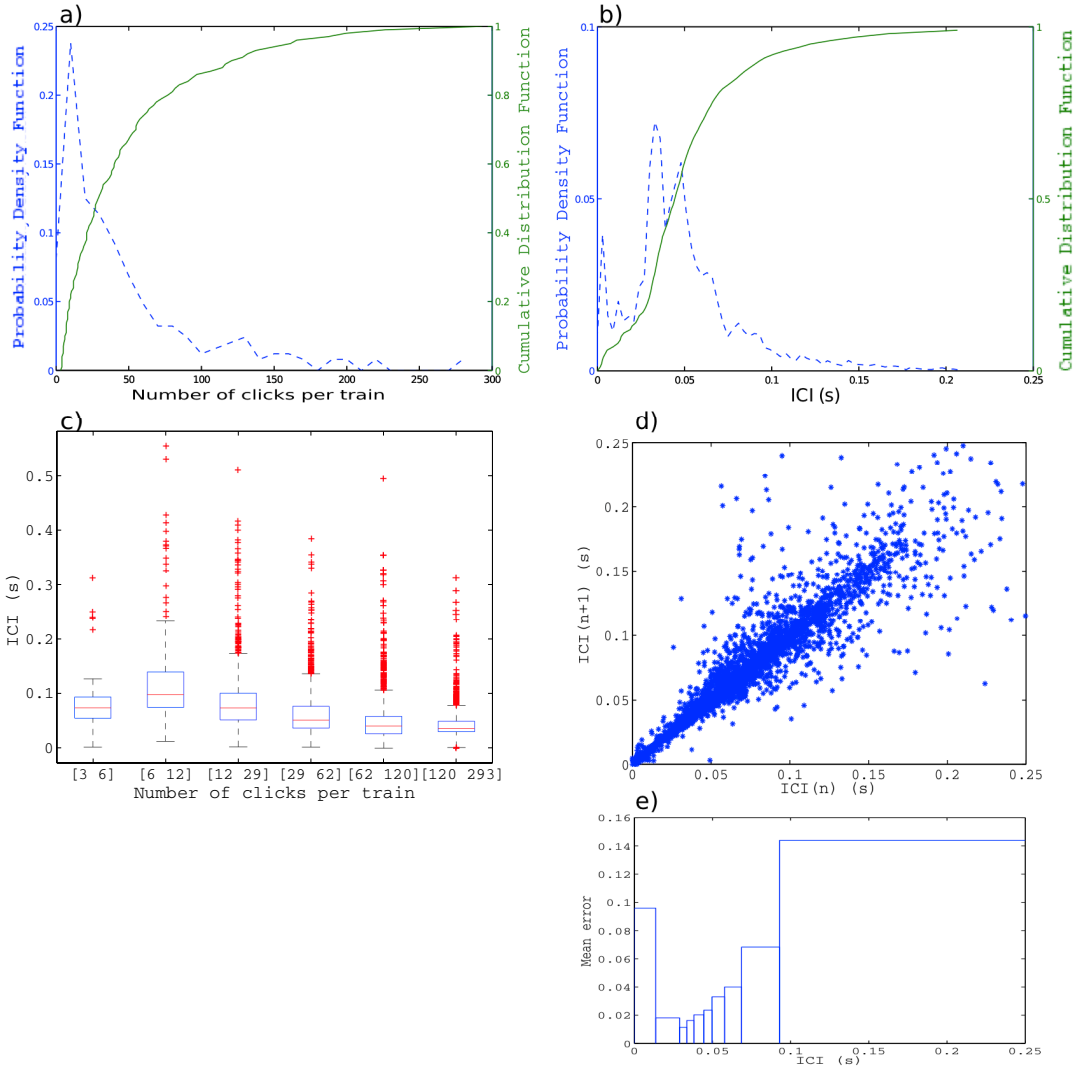

Figure 11: a) PDF (dashed line) and CDF (solid line) of the number of clicks per train. Total number of clicks: 11881. b) PDF (dashed line) and CDF (solid line) of the ICI values of the annotated click train dataset. c) Box-plot of the ICIs as a function of the number of click per train. Marks are at the 1^{st}, the 10^{th}, the 25^{th}, the 50^{th}, the 75^{th} and the 90^{th} percentiles of the CDF. Crosses are outliers. d) Relation between the ICI of the $(n+1)^{th}$ and the $(n)^{th}$ click pairs. e) Mean of the average relative jitters calculated for each ICI decile. Ignoring burst pulses, the mean of the average relative jitters increases with increasing ICI.